Coupling of quinone dynamics to proton pumping in respiratory complex I

Haapanen, Outi

2020-12-01

Haapanen , O , Reidelbach , M & Sharma , V 2020 , ' Coupling of quinone dynamics to proton pumping in respiratory complex I ' , Biochimica et Biophysica Acta. Bioenergetics , vol. 1861 , no. 12 , 148287 . https://doi.org/10.1016/j.bbabio.2020.148287

http://hdl.handle.net/10138/320183
https://doi.org/10.1016/j.bbabio.2020.148287

BBA - Bioenergetics 1861 (2020) 148287

Contents lists available at ScienceDirect

BBA - Bioenergetics

journal homepage: www.elsevier.com/locate/bbabio

Coupling of quinone dynamics to proton pumping in respiratory complex I

Outi Haapanen[a], Marco Reidelbach[a], Vivek Sharma[a,b,*]

[a] Department of Physics, University of Helsinki, Finland
[b] HiLIFE Institute of Biotechnology, University of Helsinki, Finland

ARTICLE INFO

Keywords:
Cell respiration
Molecular dynamics
Electron-proton coupling
Ubiquinone
Mitochondria

ABSTRACT

Respiratory complex I (NADH:quinone oxidoreductase) plays a central role in generating the proton electrochemical gradient in mitochondrial and bacterial membranes, which is needed to generate ATP. Several high-resolution structures of complex I have been determined, revealing its intricate architecture and complementing the biochemical and biophysical studies. However, the molecular mechanism of long-range coupling between ubiquinone (Q) reduction and proton pumping is not known. Computer simulations have been applied to decipher the dynamics of Q molecule in the ~30 Å long Q tunnel. In this short report, we discuss the binding and dynamics of Q at computationally predicted Q binding sites, many of which are supported by structural data on complex I. We suggest that the binding of Q at these sites is coupled to proton pumping by means of conformational rearrangements in the conserved loops of core subunits.

1. Introduction

Membrane-bound respiratory complex I catalyzes the reduction of ubiquinone (Q) from NADH [1,2]. It conserves the free energy of Q reduction by pumping four protons across the inner membrane of mitochondria or plasma membrane of bacteria [3,4], thereby contributing to about 40% of total proton motive force (pmf). It is a remarkable *molecular machine* that couples electron transfer (eT) reactions of ubiquinone to proton pumping as far as ~200 Å (Fig. 1). This is evidenced by the site directed mutagenesis experiments that show a point mutation in the distal antiporter-like subunit (Nqo12) of complex I affects the eT reactions in the hydrophilic module of the enzyme [5] (see also [6]). The molecular aspects of this long-range coupling remain unclear. It is unlikely to be a direct electrostatic interaction between the charge of an electron at the redox-active sites and proton in the distal pumping route. Instead the network of charged residues identified in the crystal and cryo-EM structures of complex I must play a critical role in mediating this coupling (Fig. 1). However, the question is how this is achieved at a molecular scale? How the charge reorganization at the Q binding sites is transmitted to proton pumps? And, how the charged residues that are located in the central axis undergo protonation/deprotonation reactions in a coordinated manner to provide gated routes to protons from the N-side of the membrane to the P-side? All these questions are currently major areas of experimental and computational research. The three-dimensional structural data have provided remarkable insights into the complicated architecture of complex I [7–12]. However, these *static* snapshots do not reveal how thermal motions may be important in driving the coupling between electron and proton transfer. Computer simulations based on classical and quantum chemical framework [13–20] have been important in providing mechanistic insights into how an electrostatic 'signal' from the redox-active sites travels to the proton pumping subunits involving conformational transitions.

The structural data on complex I revealed a unique ~30 Å long Q binding tunnel. It has been suggested that during complex I turnover a Q molecule would travel from the membrane phase to the N2 binding site via this tunnel, gets reduced to quinol (QH_2) and diffuse out, around 400 times per second [21]. How this occurs at an atomic scale, remains unknown, and is likely at the heart of complex I mechanism. Remarkably, part of the inner side of this unique Q chamber is highly charged whereas the other part is hydrophobic (Fig. 1). It is probably the balance between these polar and non-polar interactions between protein and hydrophobic substrate Q that drives its diffusion in and out of the tunnel. Indeed, mutation of several charged residues in and around Q tunnel region affect the binding and dynamics of Q without affecting the overall enzyme architecture [22]. Based on advanced chemical biology approaches, the single Q channel proton-pumping models of complex I have been questioned [23,24]. Instead, such approaches highlighted the presence of additional cavities or routes through which Q or its bulkier analogues travel to the active site of Q reduction.

Here, we provide a brief account of the Q binding sites observed in

* Corresponding author at: Department of Physics, University of Helsinki, Finland.
E-mail address: vivek.sharma@helsinki.fi (V. Sharma).

https://doi.org/10.1016/j.bbabio.2020.148287
Received 23 April 2020; Received in revised form 9 July 2020; Accepted 3 August 2020
Available online 07 August 2020

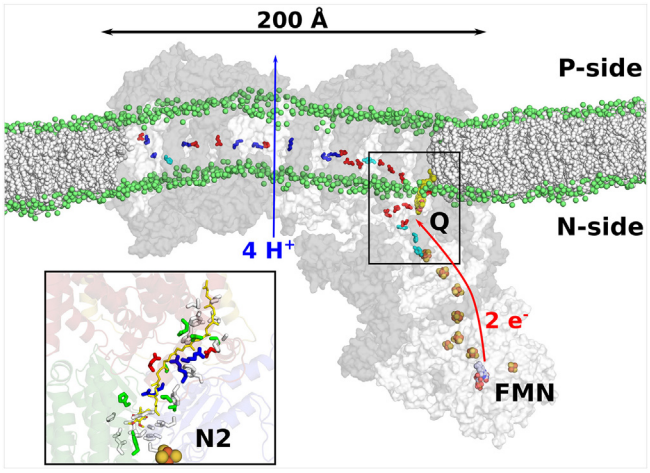

Fig. 1. Respiratory complex I from *Y. lipolytica* (PDB 6RFR) in membrane. The core subunits are shown in white surface, and accessory subunits in grey surface. The membrane is denoted with green and white spheres. Membrane bending is observed, which occurs due to relaxation of lipid bilayer around protein structure. Redox active components FMN, FeS clusters and Q are displayed. A network of charged residues connects the Q binding site to antiporter-like subunits as far as 200 Å. Inset shows a simulation snapshot with Q10 molecule bound to site 1 of *Thermus* complex I near the N2 FeS cluster. The residues from the cavity (hydrophobic – white, polar – green, acidic – red and basic - blue) surrounding the Q tail are shown. Figure is prepared with Pymol [25].

the Q tunnel based on structural and computer simulation approaches. Our analysis reveals tight coupling between the conserved loops of core subunits and dynamics of Q in the Q tunnel, which is central to the proton pumping mechanism.

2. Q binding sites in the Q tunnel – simulations and structures

Our long timescale MD simulations provided a direct view of the Q movement in the ~30 Å long Q tunnel [26]. In several MD simulations, performed on structures from two different species (mitochondrial and bacterial complex I), a Q10 molecule moved from site 1 near the N2 FeS cluster to a site near the tunnel entrance (site 5) in microseconds timescales, populating in total five transient binding sites in the Q tunnel (Fig. 2A–C). The binding of Q at these sites correspond to distinct conformational states of the protein (Fig. 2D). The opposite that is the diffusion from the site 5 to the N2 binding site 1, which would be prerequisite for eT from N2 to Q, is not seen in atomistic MD simulations due to the slower diffusion of Q in this direction. In contrast to Q10, short-tailed Q1 molecules seem to bind relatively tightly at site 1 and also diffuse out of the Q tunnel via porous cavities open to the N phase of the membrane [26]. This is likely to cause a difference in rate of catalysis between short and long-tailed substrates, as observed earlier [21].

The long timescale MD simulation data is found to be in good agreement with the free energy simulation data (umbrella sampling/weighted histogram analysis method – US/WHAM) utilizing Q1 molecule [27]. Four of the five sites observed in brute force MD simulations (1, 2, 4 and 5) are also seen in US/WHAM calculations [27]. The site 3, which is partly supported by structural data (see below), is not resolved in free energy simulations, which is probably due to insufficient sampling. In another free energy simulation work on *Thermus* enzyme with oxidized Q2/Q10 as substrates, Teixeira and Arantes [28] found 2–3 Q binding sites in the Q tunnel (resembling the sites 1, 2 and 5 in our nomenclature). In a recent work utilizing menaquinone (MQ), the natural substrate of *Thermus* enzyme, Gupta et al. [29] also observed several minima in the Q tunnel, which may correspond to sites 1, 1′ and 2 [27] (or 1, 2 and 4, respectively [26]). Overall, data from several computational studies provide a unified picture in which a number of Q binding sites exist along the Q tunnel.

Structural data from *Yarrowia* and *Thermus* complex I have been pivotal in providing detailed insights into the substrate binding sites of Q tunnel. One recent cryo EM structure of *Y. lipolytica* complex I (4.3 Å), prepared in turnover conditions, revealed a trapped substrate (decylubiquinone, DBQ) molecule [30] (site 2 in Fig. 2A). It is unclear what is the redox/protonation state of DBQ in this bound state, and also the position of its tail remains unclear, nevertheless, the location of its head group is in agreement with the brominated quinone analogue resolved in the earlier X-ray structure of complex I (3.6 Å) from the same organism (Fig. 2A) [11]. The high-resolution X-ray structure of *Thermus* complex I (3.3 Å) [7] also revealed the binding mode of a DBQ molecule and a complex I inhibitor (Piericidin), both bound near the terminal electron donor N2 FeS cluster (site 1 in Fig. 2).

More recently, a high-resolution cryo EM structure of complex I from *Y. lipolytica* (3.2 Å) [12] revealed a Q9 molecule bound at a site that was earlier predicted by computer simulations [26,27] (site 4 in Fig. 2). At this site, the Q head group is ca. 25 Å from the N2 FeS cluster, possibly representing a state with Q in transit. Another recent structural study on photosynthetic complex (3.0 Å) [34] identified a plastoquinone (PQ) molecule at a location that also resembles the site observed in MD simulations (site 3). The finding of substrate molecules at these sites clearly suggest higher occupancy and tighter binding of Q or its analogues, which may have a functional meaning (see [26]). However, we also note that the structural data are obtained at varying resolutions, from different enzymes and also the chemical nature of the bound substrate molecules is different. Nevertheless, overall structural homology between structures, the conserved location and architecture of the Q tunnel and key residues in it, as well as consistency with the computer simulation data, supports the notion that Q binding sites may be conserved in complexes from several different species.

Overall, the Q binding positions in the Q tunnel (1–4) are supported by the structural data, except for site 5, which is yet to be observed experimentally (Fig. 2A). The latter site is closer to the Q tunnel entrance, and binding of a Q molecule at this location may strongly depend on lipidic conditions, and novel approaches of membrane protein characterization in nanodiscs, may for example, be beneficial in trapping Q at this site. It also remains to be seen if the proposed low energy site 5 corresponds to the experimental data that show a stoichiometry of one tightly-bound Q per complex I [35,36]. Importantly, site 5 is next to the short horizontal helix between transmembrane helices (TMH) 1 and 2 of ND1/Nqo8 subunit, which harbors a well-known mitochondrial mutation (Ala54Thr, *Yarrowia* numbering) [37].

3. Q reduction and dynamics in the cavity is coupled to the conformational dynamics of conserved loops

Earlier based on multiscale computational approaches, it has been shown that the reduction of Q by two electrons results in local proton transfers from conserved His38 and Tyr87 of Nqo4 subunit, forming QH_2 and two proton vacancies (on Tyr87 and His38) [31]. Classical MD simulations of these states, that is before and after reduction-coupled protonation, showed remarkable changes in the dynamics of conserved residues in β1-β2 loop of Nqo4 subunit. The neutral His38 moves closer to anionic Tyr87, which is coupled to the departure of QH_2 from site 1 to site 2. This is also seen in free energy calculations in which QH_2 has minima at site 2, whereas oxidized Q prefers to bind at site 1 [27]. The results are also corroborated by long timescale simulations of Q and QH_2 in which the movement of substrate between sites 1 and 2 is coupled to the dynamics of β1-β2 loop [26]. Indeed, structures of complexes with Q or its analogues modeled at these sites reveal large scale changes in the β1-β2 loop [38]. We think that despite uncertainties in modeling of flexible loops and sidechains in structural biology experiments, the loop conformations and Q positions obtained after refinements may represent functionally relevant states. And,

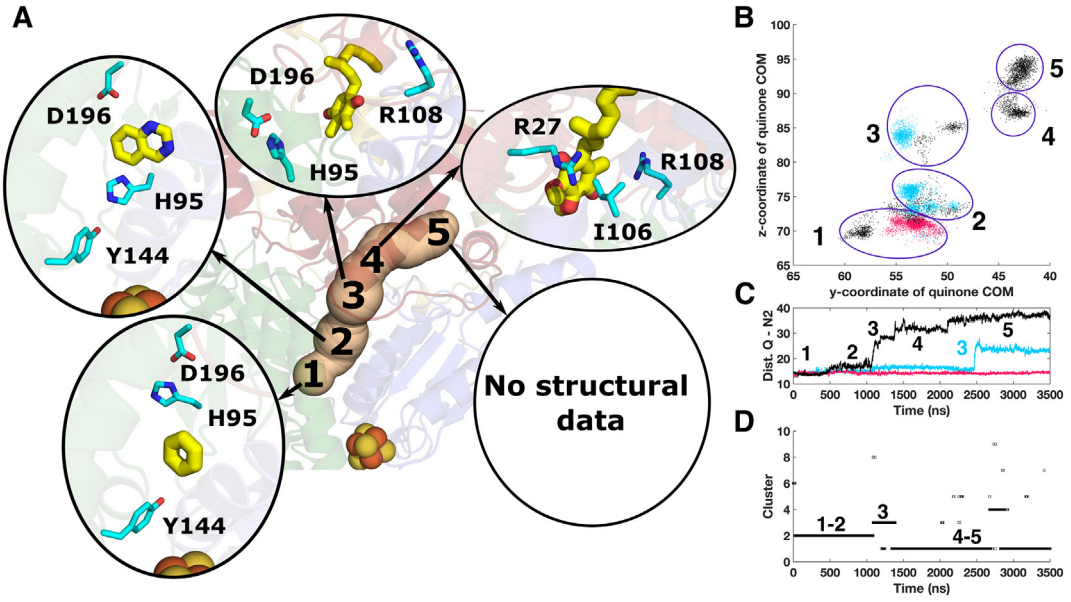

Fig. 2. (A) Five Q binding sites (1–5) identified in the Q tunnel based on computer simulations performed in ref. [26]. Sites 1–4 are supported by the structural data on complex I (see text). A Q head group ring is modeled at site 1 based on PDB 4HEA (see [18,31]). Site 2 shows a quinone analogue (PDB 4WZ7). The recently solved cryo EM structure of photosynthetic complex I (PDB 6KHJ) shows a plastoquinone (PQ) in site 3 region. Furthermore, a Q9 molecule has recently been observed at site 4 (PDB 6RFR). There is no structural support for the computationally predicted site 5. Residue numbering is based on *Y. lipolytica* complex I. Figure is prepared with Pymol [25]. (B) The y/z coordinates of Q head group center of mass (COM) are plotted from three independent simulations of *Bos taurus* (PDB 5LC5) complex I. The scatter plot reveals five distinct Q binding sites in the positive z-direction (marked in circles), which corresponds to Q movement from site 1 to 5 along the membrane normal. The simulation trajectories were aligned (Cα-atoms of protein) to remove rotation and translation of the simulation box. (C) Time evolution of the same *B.t.* simulations as in panel A. Distance between COM of N2 FeS cluster and quinone ring also reveals Q binding sites in the Q tunnel. (D) Time evolution of clusters formed during the simulation in which Q moves through the entire tunnel (black trace in panel C). Comparison with Q movement (panel C) reveals distinct conformational states protein visits during Q movement (clusters 2, 3 and 1 corresponds to sites 1/2, 3 and 4/5, respectively). Clustering of simulation trajectory was performed using GROMACS [32] clustering tool with gromos method [33]. Quinone atoms and Cα-atoms of subunits 49-kD, PSST and ND1 were used for clustering with an RMSD cutoff of 3 Å.

computer simulations in several different redox/protonation states provide a more meaningful interpretation of these data.

The extensive MD data on Q dynamics [26] were subjected to network-based approaches [39] to learn about the conformational changes that would occur when Q diffuses between two sites (1 and 5) in the Q tunnel. We focused on the dynamics of four loops (TMH5-6 loop of Nqo8/ND1 subunit, Nqo7/ND3 loop, His34/55 and His38/59 carrying β1-β2 loop of Nqo4/49 kD and central loop of Nqo6/PSST) that have been identified to be central in the mechanism of complex I [11,22,40]. Note, in this analysis we study conformational changes that take place upon Q binding and dynamics, and no change in protonation/redox states are accounted for, which have earlier been studied by means of continuum electrostatic approaches (see e.g. [27] on how pK_a changes occur upon Q dynamics). We find in both bacterial and mitochondrial complex I simulations, the correlation pathways (residues showing correlated motions) between conserved loops are shorter and stronger when Q binds near N2 (sites 1 and 2) (Fig. 3). However, when Q is at the entrance site 5, these correlations weaken, which suggests that the coupled dynamics of conserved loops allow efficient trapping of Q at sites near N2 for favourable eT. We think that having flexible loops instead of relatively rigid secondary structure facing the cavity is better for the highly flexible and dynamic redox cofactor Q that travels in and out of the cavity.

A more detailed look at the correlation networks shows that when Q is bound at site 1 several correlation pathways form between 49 kD and ND1 loops, which are lost upon transfer of Q to site 5. Interestingly, this loss of correlation pathways between 49 kD and ND1 loops results in gain of correlation pathways towards the ND3 loop (Fig. 4). A similar rearrangement of pathways is also seen between 49 kD and PSST, and ND3 loops. This suggests that the loops of 49 kD, ND1 and PSST subunits that face the cavity may play a role in Q binding, whereas ND3 loop assists in unlatching the Q from the N2 binding site by a possible combination of conformational and electrostatic rearrangements.

4. Energetics of Q binding and dynamics

Even though overlapping Q binding sites are observed in several computational studies [26–29], some subtle energetic differences are puzzling. Warnau et al. [27] and Teixeira and Arantes [28] utilized small and long-tailed Q analogues and observed a stable site near the entrance of the Q tunnel (site 5 in Fig. 2). This site is also observed in unbiased simulations [26] in which a Q10 molecule after diffusing in the entire tunnel binds in a stable manner at the latter site. Interestingly, this minimum is not observed in the recent work by Gupta et al. [29], who utilized MQ, the natural substrate of *Thermus* complex I. Instead, MQ preferentially binds to site 1 in their work, which is necessary for electron transfer from N2. Even though *Thermus* enzyme is fully active with DBQ [7], the differences in free energy profiles for Q and MQ are puzzling. If they represent a real scenario, this may point to how evolution fine-tuned enzyme architecture to efficiently utilize one substrate over another. For instance, somewhat weaker binding of Q at site 1 may be compensated by its higher redox potential (ca. 100 mV) in contrast to stronger binding of MQ (redox potential, ca. -80 mV). Further work is required to resolve these issues.

Interestingly, in none of the structures solved to date a long-tailed Q10 or menaquinone is found at the binding site near N2 (site 1). The reasons for this are also not fully clear, however, this would be in partial agreement with the observations from modeling and simulation work. For example, the data from long timescale MD simulations [26] and free energy calculations [27,28] show that the binding of an oxidized Q molecule at the obligatory redox active site near N2 is somewhat weaker in comparison to the site near the entrance of the Q tunnel

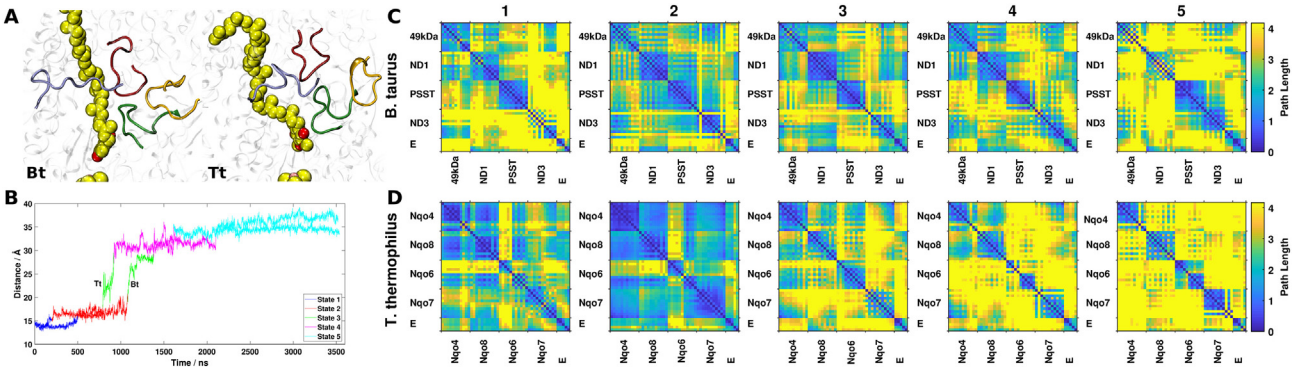

Fig. 3. (A) Loops from subunits 49 kD/Nqo4 (green), ND1/Nqo8 (red), PSST/Nqo6 (ice blue), and ND3/Nqo7 (yellow) in complex I from *Bos taurus* (Bt) and *Thermus thermophilus* (Tt) with Q at site 1 are shown. Van der Waals representation for Q and N2 FeS cluster. Figure is prepared with VMD [41]. (B) Distance between the center-of-mass of the six carbon atoms of the Q head group ring and the center-of-mass of the N2 FeS cluster in *B. taurus* and *T. thermophilus* MD simulations. Binding of Q at sites 1, 2, 3, 4, and 5 are depicted in blue, red, green, magenta, and cyan, respectively. Heatmaps depicting the optimal correlation path lengths (minimal sum of logarithmic correlation values) between the loops and E channel residues in bovine (C) and *Thermus* (D) enzymes. Short correlation pathways (stronger correlation) depicted in blue and long correlation pathways (weaker correlation) depicted in yellow. The following residues of loops of 49 kD/Nqo4 (51–61/30–40), ND1/Nqo8 (199–209/220–230), PSST/Nqo6 (69–79/60–70), and ND3/Nqo7 (33–43/40–50) were considered in the analysis. The E channel residues in *B. taurus* are E143, E192, E227 (ND1) and D66, E68 (ND3), whereas in *T. thermophilus* these are E163, E213, E248 (Nqo8) and D72, E74 (Nqo7). The correlation pathways are calculated using NetworkView [39] and an in-house implementation based on Floyd-Warshall algorithm [42,43].

(site 5) and nearly similar in energy with respect to the membrane. One of the likely reasons for the weaker binding at the N2 site relative to the entrance sites is that the hydrophobic tail of Q10 passes through a rather hydrophilic and charged region of the Q tunnel (Fig. 1 inset), which is energetically unfavorable. On the other hand, the flexible hydrophobic tail of Q10 mixes well with the lipid tails that partly stabilizes its position at site 5, at the entrance of the Q tunnel (Q1 is also stable).

Free energy calculations with quinones of different tail lengths showed barriers of the order of ca. 10 kcal/mol for the movement of Q towards the N2 binding from the site at the entrance. This corresponds to ca. tens to hundreds of microseconds timescale for a Q molecule to travel towards the N2 binding site. As discussed earlier [27], any variations in energy barriers may make Q dynamics in the tunnel rate limiting (cf. [21]). Therefore, to overcome these limitations of weaker binding at the N2 site and possible slower dynamics in the tunnel, additional mechanistic ideas have been circulated. One possibility is that despite its weaker binding, Q is trapped at the N2 binding site by a fast electron transfer from N2 converting it to an anionic semiquinone [27], similar to the kinetic trapping of oxygen in cytochrome *c* oxidase [44]. Indeed, steered MD data show that anionic SQ binds relatively tightly in the tunnel [27], and would not leave the reactive site prior to accepting the next electron forming quinol (in coupling to intra-protein proton transfer).

5. Two quinones and one enzyme

To overcome potential high energy barriers in the Q tunnel, a model has been proposed involving two Q molecules, in which one Q acts as an electron-shuttler in the Q tunnel and transfers electrons from N2 to a secondary replaceable Q [45]. There are arguments in favor and against this model. For instance, complex I structure trapped in turnover conditions shows besides the bound substrate molecule at site 2 (DBQ), a strong electron density ca. 25 Å from the N2 center, which could potentially represent a Q molecule [12]. This suggests that two small Q molecules (or one big and one small) can occupy the Q tunnel during

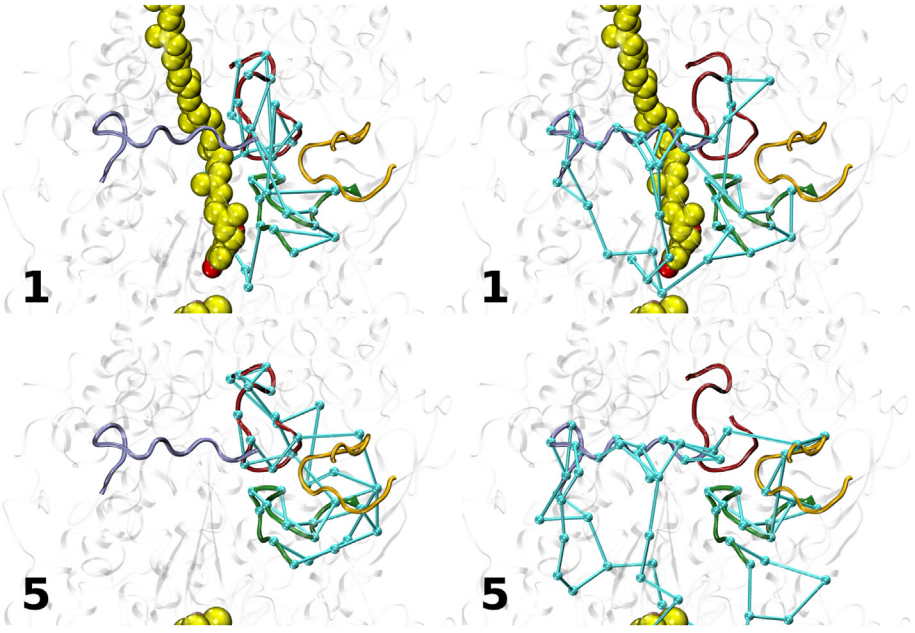

Fig. 4. Optimal correlation pathways (cyan) connecting the 49 kD and ND1 loops (left) and 49 kD and PSST loops (right) in complex I from *B. taurus* for Q at positions 1 (top) and 5 (bottom). The 49 kD, ND1, PSST, and ND3 loops are depicted in green, red, ice blue, and yellow, respectively. Van der Waals representation for Q and N2 FeS cluster. Figure is prepared with VMD [41].

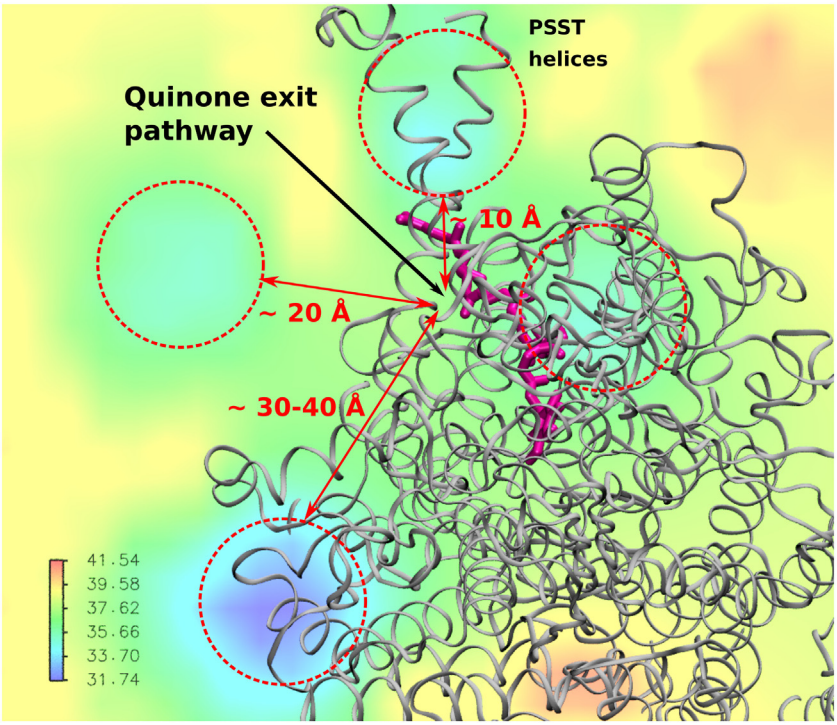

Fig. 5. Variation in membrane thickness adjacent to protein shown by a 2D thickness map (scale in Å). The regions where membrane thickness is lower are marked by dotted circles and their approximate location from the Q tunnel entrance. Q is shown in magenta color. The membrane thickness is calculated with MEMBPLUGIN [53] tool using the 1 μs MD simulation of *Yarrowia* complex I [12]. Only core subunits are shown as grey ribbons, and the view is from the matrix/N-side of the membrane. Figure is prepared with VMD [41].

turnover. However, the question is does this represent a catalytically relevant state in which two Q molecules can exchange electrons (and protons)? One possibility is that a small Q molecule shuttles between sites 1–3 and delivers electrons to Q10 bound at sites 4/5, which then departs the Q tunnel to be replaced by a new oxidized Q. However, how will this be achieved with two full length Q10 molecules that would occupy the Q tunnel at the same time? In this case, tail of the Q10 molecule bound at the N2 binding site has to pass through one of the many cavities observed in the membrane-facing surface of the protein (see [26]), in order to prevent its clash with the Q molecule bound at the entrance. For a potential inter-quinone electron transfer reaction between the head group of two Q molecules, they must approach the electron transfer distance of ca. 14 Å or less. Moreover, to achieve this, transient binding sites must exist in the Q tunnel with potential access to proton transfer pathways [26]. Some ideas regarding this have been discussed in the literature [13,45], and clearly more work is needed to prove or disprove this hypothesis of "Q2Q" eT.

There are not many enzyme families that catalyze inter-quinone electron transfer. One of them is photosystem II, in which eT occurs from a tightly bound plastoquinone QA to an exchangeable one, QB (mediated by a non-heme iron) [46]. Interestingly, in the structure of NDH-2 from *Saccharomyces cerevisiae*, two Q molecules are observed within eT distance to each other, prompting a possibility of inter-quinone redox reaction [47,48]. However, it remains to be proven experimentally that this is part of NDH-2 turnover or just an artifact of high Q concentration used in the structural study [49]. Nevertheless, the notion of a possible Q2Q eT in complex I is an interesting proton pumping model in the light of available structural, biochemical and computational data, and is an active area of research.

6. Role of lipids in Q binding and dynamics

It is clear that during a single complex I turnover an oxidized quinone molecule undergoes reduction and protonation, and is exchanged with an oxidized one. The structurally characterized Q binding channel, through which quinone transits, opens to the lipid membrane. This suggests that the entry and exit of a Q molecule must be occurring in tight coupling to the lipid-protein interactions. In fact, the highly tilted tails of lipids at the tunnel entrance may directly contribute to the dynamics of Q in and out of the Q tunnel [12]. The dynamics of Q in different types of lipid membranes have been studied earlier by atomistic MD simulations [50,51]. Coarse grained MD data on *Thermus* complex I suggested cardiolipin-based enhancement of Q binding at the site near N2 cluster (sites 1/2) [52]. Interestingly, in the recent cryo EM structure of mitochondrial complex I , we observed a unique lipid-protein arrangement that may also be important to Q binding and dynamics at the membrane-protein interface. We found based on structural data and atomistic MD simulations that the thickness of the lipid-bilayer is reduced adjacent to the protein surface (Fig. 5). This is primarily caused by the rearrangement of lipid tails to accommodate the unique architecture of amphipathic helices of the protein subunits [12].

We envisage that this variation in bilayer thickness may play a role in the dynamics of Q near the vicinity of protein. Flipping of Q molecules from one leaflet to another is necessary for cell respiration, and some kinetic enhancement in that may be achieved with the reduced bilayer thickness. In addition to the reduced thickness, data also show bending of the lipid membrane [12]. It is known that the bending of lipid membranes in the vicinity of enzyme is energetically costly [54]. Therefore, the question is why the enzyme invests energy in membrane deformation? This change in membrane morphology may drive Q molecules towards the Q channel, and such aspects can be studied by a combination of theoretical and experimental approaches in the future.

Declaration of competing interest

The authors declare that they have no known competing financial interests or personal relationships that could have appeared to influence the work reported in this paper.

Acknowledgements

VS acknowledges helpful discussions with Volker Zickermann, Mårten Wikström, Abhishek Singharoy and Chitrak Gupta. We thank the Academy of Finland, the Sigrid Jusélius Foundation and the University of Helsinki for financial support. We are grateful to the Center for Scientific Computing (CSC), Finland for continuous

computational support of highest quality. We acknowledge PRACE for awarding us access to MareNostrum at the Barcelona Supercomputing Center (BSC), Spain.

References

[1] U. Brandt, Energy converting NADH: quinone oxidoreductase (complex I), Annu. Rev. Biochem. 75 (2006) 69–92.
[2] L.A. Sazanov, A giant molecular proton pump: structure and mechanism of respiratory complex I, Nat. Rev. Mol. Cell Biol. 16 (2015) 375–388.
[3] M. Wikström, Two protons are pumped from the mitochondrial matrix per electron transferred between NADH and ubiquinone, FEBS Lett. 169 (1984) 300–304.
[4] A. Galkin, V. Grivennikova, A. Vinogradov, →H+/2e stoichiometry in NADH-quinone reductase reactions catalyzed by bovine heart submitochondrial particles, FEBS Lett. 451 (1999) 157–161.
[5] E. Nakamaru-Ogiso, M.-C. Kao, H. Chen, S.C. Sinha, T. Yagi, T. Ohnishi, The membrane subunit NuoL (ND5) is involved in the indirect proton pumping mechanism of Escherichia coli complex I, J. Biol. Chem. 285 (2010) 39070–39078.
[6] L. Euro, G. Belevich, M.I. Verkhovsky, M. Wikström, M. Verkhovskaya, Conserved lysine residues of the membrane subunit NuoM are involved in energy conversion by the proton-pumping NADH: ubiquinone oxidoreductase (complex I), Biochimica et Biophysica Acta (BBA)-Bioenergetics 1777 (2008) 1166–1172.
[7] R. Baradaran, J.M. Berrisford, G.S. Minhas, L.A. Sazanov, Crystal structure of the entire respiratory complex I, Nature 494 (2013) 443–448.
[8] K. Fiedorczuk, J.A. Letts, G. Degliesposti, K. Kaszuba, M. Skehel, L.A. Sazanov, Atomic structure of the entire mammalian mitochondrial complex I, Nature 538 (2016) 406–410.
[9] J. Zhu, K.R. Vinothkumar, J. Hirst, Structure of mammalian respiratory complex I, Nature 536 (2016) 354–358.
[10] J.N. Blaza, K.R. Vinothkumar, J. Hirst, Structure of the deactive state of mammalian respiratory complex I, bioRxiv 26 (2017) 165753312–319.
[11] V. Zickermann, C. Wirth, H. Nasiri, K. Siegmund, H. Schwalbe, C. Hunte, U. Brandt, Mechanistic insight from the crystal structure of mitochondrial complex I, Science 347 (2015) 44–49.
[12] K. Parey, O. Haapanen, V. Sharma, H. Köfeler, T. Züllig, S. Prinz, K. Siegmund, I. Wittig, D.J. Mills, J. Vonck, High-resolution cryo-EM structures of respiratory complex I: mechanism, assembly, and disease, Science Advances 5 (2019) eaax9484.
[13] O. Haapanen, V. Sharma, A modeling and simulation perspective on the mechanism and function of respiratory complex I, Biochimica et Biophysica Acta (BBA)-Bioenergetics 1859 (2018) 510–523.
[14] V.R. Kaila, Long-range proton-coupled electron transfer in biological energy conversion: towards mechanistic understanding of respiratory complex I, J. R. Soc. Interface 15 (2018) 20170916.
[15] G. Hummer, M. Wikström, Molecular simulation and modeling of complex I, Biochimica et Biophysica Acta (BBA)-Bioenergetics 1857 (2016) 915–921.
[16] A. Djurabekova, O. Haapanen, V. Sharma, Proton motive function of the terminal antiporter-like subunit in respiratory complex I, Biochimica et Biophysica Acta (BBA)-Bioenergetics 1861 (2020) 148185.
[17] A. Di Luca, A.P. Gamiz-Hernandez, V.R. Kaila, Symmetry-related proton transfer pathways in respiratory complex I, Proc. Natl. Acad. Sci. 114 (2017) E6314–E6321.
[18] O. Haapanen, V. Sharma, Role of water and protein dynamics in proton pumping by respiratory complex I, Sci. Rep. 7 (2017) 7747.
[19] P. Tan, Z. Feng, L. Zhang, T. Hou, Y. Li, The mechanism of proton translocation in respiratory complex I from molecular dynamics, Journal of Receptors and Signal Transduction 35 (2015) 170–179.
[20] U. Khaniya, C. Gupta, X. Cai, J. Mao, D. Kaur, Y. Zhang, A. Singharoy, M. Gunner, Hydrogen bond network analysis reveals the pathway for the proton transfer in the E-channel of *T. thermophilus* complex I, Biochimica et Biophysica Acta (BBA)-Bioenergetics 1861 (2020) 148240.
[21] J.G. Fedor, A.J. Jones, A. Di Luca, V.R. Kaila, J. Hirst, Correlating kinetic and structural data on ubiquinone binding and reduction by respiratory complex I, Proc. Natl. Acad. Sci. 201714074 (2017).
[22] E.G. Yoga, O. Haapanen, I. Wittig, K. Siegmund, V. Sharma, V. Zickermann, Mutations in a conserved loop in the PSST subunit of respiratory complex I affect ubiquinone binding and dynamics, Biochimica et Biophysica Acta (BBA)-Bioenergetics 1860 (2019) 573–581.
[23] S. Uno, H. Kimura, M. Murai, H. Miyoshi, Exploring the quinone/inhibitor-binding pocket in mitochondrial respiratory complex I by chemical biology approaches, J. Biol. Chem. 294 (2019) 679–696.
[24] S. Uno, T. Masuya, K. Shinzawa-Itoh, J. Lasham, O. Haapanen, T. Shiba, D.K. Inaoka, V. Sharma, M. Murai, H. Miyoshi, Oversized ubiquinones as molecular probes for structural dynamics of the ubiquinone reaction site in mitochondrial respiratory complex I, J. Biol. Chem. 295 (2020) 2449–2463.
[25] L. Schrodinger, The PyMOL molecular graphics system, Version, 1 (2019) r1, 2010.
[26] O. Haapanen, A. Djurabekova, V. Sharma, Role of second quinone binding site in proton pumping by respiratory complex I, Frontiers in Chemistry 7 (2019) 221.
[27] J. Warnau, V. Sharma, A.P. Gamiz-Hernandez, A. Di Luca, O. Haapanen, I. Vattulainen, M. Wikström, G. Hummer, V.R. Kaila, Redox-coupled quinone dynamics in the respiratory complex I, Proc. Natl. Acad. Sci. 115 (2018) E8413–E8420.
[28] M.H. Teixeira, G.M. Arantes, Balanced internal hydration discriminates substrate binding to respiratory complex I, Biochimica et Biophysica Acta (BBA)-Bioenergetics 1860 (2019) 541–548.
[29] C. Gupta, U. Khaniya, C.K. Chan, F. Dehez, M. Shekhar, M.R. Gunner, L. Sazanov, C. Chipot, A. Singharoy, Charge transfer and chemo-mechanical coupling in respiratory complex I, J. Am. Chem. Soc. 142 (2020) 9220–9230.
[30] K. Parey, U. Brandt, H. Xie, D.J. Mills, K. Siegmund, J. Vonck, W. Kühlbrandt, V. Zickermann, Cryo-EM structure of respiratory complex I at work, Elife 7 (2018) e39213.
[31] V. Sharma, G. Belevich, A.P. Gamiz-Hernandez, T. Róg, I. Vattulainen, M.L. Verkhovskaya, M. Wikström, G. Hummer, V.R. Kaila, Redox-induced activation of the proton pump in the respiratory complex I, Proc. Natl. Acad. Sci. 112 (2015) 11571–11576.
[32] M.J. Abraham, T. Murtola, R. Schulz, S. Páll, J.C. Smith, B. Hess, E. Lindahl, GROMACS: high performance molecular simulations through multi-level parallelism from laptops to supercomputers, SoftwareX 1 (2015) 19–25.
[33] X. Daura, K. Gademann, B. Jaun, D. Seebach, W.F. Van Gunsteren, A.E. Mark, Peptide folding: when simulation meets experiment, Angew. Chem. Int. Ed. 38 (1999) 236–240.
[34] X. Pan, D. Cao, F. Xie, F. Xu, X. Su, H. Mi, X. Zhang, M. Li, Structural basis for electron transport mechanism of complex I-like photosynthetic NAD (P) H dehydrogenase, Nat. Commun. 11 (2020) 1–11.
[35] M. Verkhovsky, D.A. Bloch, M. Verkhovskaya, Tightly-bound ubiquinone in the *Escherichia coli* respiratory complex I, Biochimica et Biophysica Acta (BBA)-Bioenergetics 1817 (2012) 1550–1556.
[36] K. Shinzawa-Itoh, J. Seiyama, H. Terada, R. Nakatsubo, K. Naoki, Y. Nakashima, S. Yoshikawa, Bovine heart NADH − ubiquinone oxidoreductase contains one molecule of ubiquinone with ten isoprene units as one of the cofactors, Biochemistry 49 (2009) 487–492.
[37] N. Howell, L. Bindoff, D. McCullough, I. Kubacka, J. Poulton, D. Mackey, L. Taylor, D. Turnbull, Leber hereditary optic neuropathy: identification of the same mitochondrial ND1 mutation in six pedigrees, Am. J. Hum. Genet. 49 (1991) 939.
[38] E.G. Yoga, H. Angerer, K. Parey, V. Zickermann, Respiratory complex I–mechanistic insights and advances in structure determination, Biochimica et Biophysica Acta (BBA)-Bioenergetics 1861 (2020) 148153.
[39] J. Eargle, Z. Luthey-Schulten, NetworkView: 3D display and analysis of protein·RNA interaction networks, Bioinformatics 28 (2012) 3000–3001.
[40] A. Cabrera-Orefice, E.G. Yoga, C. Wirth, K. Siegmund, K. Zwicker, S. Guerrero-Castillo, V. Zickermann, C. Hunte, U. Brandt, Locking loop movement in the ubiquinone pocket of complex I disengages the proton pumps, Nat. Commun. 9 (2018) 1–10.
[41] W. Humphrey, A. Dalke, K. Schulten, VMD: visual molecular dynamics, J. Mol. Graph. 14 (1996) 33–38.
[42] R.W. Floyd, Algorithm 97: shortest path, Commun. ACM 5 (1962) 345.
[43] S. Warshall, A theorem on boolean matrices, Journal of the ACM (JACM) 9 (1962) 11–12.
[44] M.I. Verkhovsky, J.E. Morgan, A. Puustinen, M. Wikstrom, Kinetic trapping of oxygen in cell respiration, Nature 380 (1996) 268.
[45] M. Wikstrom, V. Sharma, V.R. Kaila, J.P. Hosler, G. Hummer, New perspectives on proton pumping in cellular respiration, Chem. Rev. 115 (2015) 2196–2221.
[46] Y. Umena, K. Kawakami, J.-R. Shen, N. Kamiya, Crystal structure of oxygen-evolving photosystem II at a resolution of 1.9 Å, Nature 473 (2011) 55–60.
[47] Y. Feng, W. Li, J. Li, J. Wang, J. Ge, D. Xu, Y. Liu, K. Wu, Q. Zeng, J.-W. Wu, Structural insight into the type-II mitochondrial NADH dehydrogenases, Nature 491 (2012) 478–482.
[48] A. Godoy-Hernandez, D.J. Tate, D.G. McMillan, Revealing the membrane-bound catalytic oxidation of NADH by the drug target type-II NADH dehydrogenase, Biochemistry 58 (2019) 4272–4275.
[49] J.N. Blaza, H.R. Bridges, D. Aragão, E.A. Dunn, A. Heikal, G.M. Cook, Y. Nakatani, J. Hirst, The mechanism of catalysis by type-II NADH: quinone oxidoreductases, Sci. Rep. 7 (2017) 1–11.
[50] V.V. Galassi, G.M. Arantes, Partition, orientation and mobility of ubiquinones in a lipid bilayer, Biochimica et Biophysica Acta (BBA)-Bioenergetics 1847 (2015) 1560–1573.
[51] P. Kaurola, V. Sharma, A. Vonk, I. Vattulainen, T. Rog, Distribution and dynamics of quinones in the lipid bilayer mimicking the inner membrane of mitochondria, Biochimica et Biophysica Acta (BBA)-Biomembranes 1858 (2016) 2116–2122.
[52] A. Jussupow, A. Di Luca, V.R. Kaila, How cardiolipin modulates the dynamics of respiratory complex I, Science Advances 5 (2019) eaav1850.
[53] R. Guixà-González, I. Rodriguez-Espigares, J.M. Ramírez-Anguita, P. Carrió-Gaspar, H. Martinez-Seara, T. Giorgino, J. Selent, MEMBPLUGIN: studying membrane complexity in VMD, Bioinformatics 30 (2014) 1478–1480.
[54] W. Zhou, G. Fiorin, C. Anselmi, H.A. Karimi-Varzaneh, H. Poblete, L.R. Forrest, J.D. Faraldo-Gómez, Large-scale state-dependent membrane remodeling by a transporter protein, Elife 8 (2019) e50576.